

International Journal of Vehicle Information and Communication Systems

ISSN online: 1741-8208 - ISSN print: 1471-0242
<https://www.inderscience.com/ijvics>

Research on automatic early warning of UAV attitude abnormal state based on MEMS sensor

Xiaoqiang Wang

DOI: [10.1504/IJVICS.2023.10056035](https://doi.org/10.1504/IJVICS.2023.10056035)

Article History:

Received:	20 December 2022
Last revised:	29 January 2023
Accepted:	07 February 2023
Published online:	20 June 2023

Research on automatic early warning of UAV attitude abnormal state based on MEMS sensor

Xiaoqiang Wang

Chinese-German College of Engineering,
Shanghai Technical Institute of Electronics Information,
Fengxian District, Shanghai, China
Email: 20220079@stiei.edu.cn

Abstract: The Unmanned Aerial Vehicle's (UAV) attitude control is crucial to the success of the mission. On the basis of this, the paper suggests a paradigm for autonomous early warning of improper UAV attitude based on MEMS sensors. To obtain early warning of anomalous UAV attitude, the model solves UAV attitude using the quaternion approach and employs a fading Kalman filter to correct for MEMS gyroscope inaccuracy. The simulation test demonstrates that in the static state, the errors of the drone's pitch angle and roll angle are within 0.2° , and the heading angle error is about 0.5° . In the high manoeuvring state, the errors of the UAV's pitch angle and roll angle are all within 0.5° , and the mean value of the heading angle error is also controlled within 2° . The experiment achieves high-precision automated warning of aberrant attitude by filtering the fading Kalman filter to correct the random error of the UAV gyroscope. It also increases the precision with which human motion is measured. The suggested approach promotes the growth of the UAV sector.

Keywords: MEMS sensor; unmanned aerial vehicle; abnormal attitude; fading Kalman filter; gyro error; quaternion; Allan variance; early warning.

Reference to this paper should be made as follows: Wang, X. (2023) 'Research on automatic early warning of UAV attitude abnormal state based on MEMS sensor', *Int. J. Vehicle Information and Communication Systems*, Vol. 8, Nos. 1/2, pp.66–84.

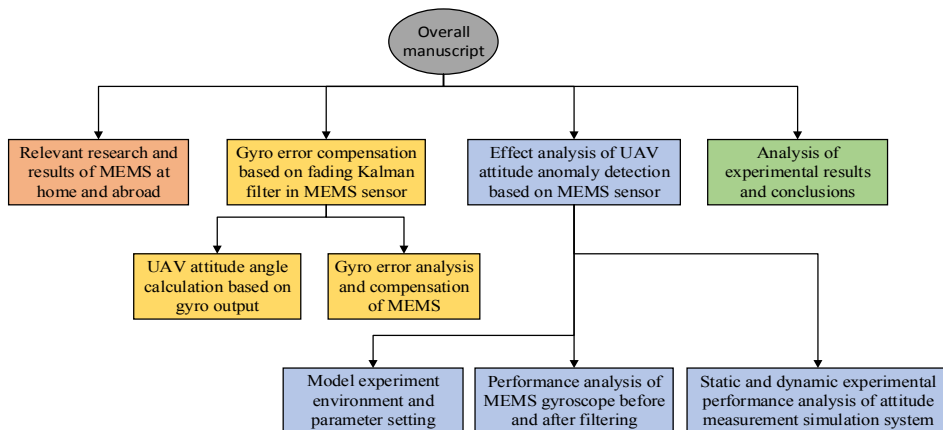
Biographical notes: Xiaoqiang Wang is an Associate Professor. He Graduated from Chang'an University in 2009, major in Environmental Engineering, with a Master's degree. Now, he is working in Shanghai Technical Institute of Electronics & Information. He mainly engages in the research of civil drone application technology. So far, He has published 7 papers and participated in 3 projects.

1 Introduction

The micro-electro-mechanical and micro-electronic technology has been developing continuously, and the Micro-Electro-Mechanical System (MEMS) is one of the crystallisation products of this technology (Li et al., 2019). MEMS is composed of the latest modern information technology and micro-processing technology, such as ultra-high-precision machining technology and micro-processing technology of semiconductor

integrated circuits. In the field of micro-engineering, micro-stereo lithography has become a promising manufacturing process. The ladder effect on the side surface of 3D micro-structures has been reduced using a variety of technologies, and methods relevant to different kinds of microstructures have been developed (Bhole, 2022). The outcomes of releasing microstructure without static friction may be obtained by using sublimation drying and release technology to the static friction effect in the MEMS post-treatment process. This creates a novel method for the post-treatment of microarray structure (Bhole and Kale, 2022). The internal structure of MEMS is generally micron or even nanometre scale, and it is an independent intelligent system. In practical applications, MEMS has many advantages such as small size, low cost, fast response, easy integration and high intelligence, which occupies an important position in the current research field of inertial technology (Stepanovsky, 2019). The three accuracy indications for MEMS inertial sensors – high, medium and low – are based on measurement accuracy standards and are utilised extensively in a variety of industries. In the field of unmanned aerial vehicles, MEMS inertial sensors can be used for positioning, detection and analysis of unmanned aerial vehicles, but the current accuracy of MEMS has not yet reached the index requirements of high-precision navigation systems. Without correct and timely judgments, it may lead to UAV accidents (Ye et al., 2019). In order to make the UAV have more lasting characteristics during operation, the UAV needs to detect its own status. To increase the precision of UAV attitude measurement and accomplish the impact of automated warning of UAV attitude abnormal condition, the study employs fading Kalman filter to correct the random error of MEMS gyroscope. The essence of the proposed method is to use the sensing accuracy of MEMS to detect the attitude of UAV. The sensor can assess the UAV's attitude angle, establish its coordinate system and provide early warning based on the magnitude of the UAV angle. It is challenging for the UAV attitude anomaly early warning system to employ traditional techniques for early warning due to numerous random faults in the inertial sensors. By improving the detection accuracy of the sensor, the research innovates from the early warning system to the prediction of UAV attitude, thus realising the effective early warning of UAV attitude anomalies. The overall structure of the article is shown in Figure 1.

Figure 1 Overall structure of the article



The theoretical contribution of this study is to establish different coordinate systems of UAV, and calculate the attitude angle of UAV through coordinate system transformation. The impact of the UAV gyroscope's random error on the early warning model is also examined using Allen variance. Finally, the fading Kalman filter is used to compensate the error, thus improving the measurement accuracy of UAV gyro. This research innovates the UAV early warning mode, and realises the UAV attitude early warning mainly through the angle change of UAV attitude. This early warning method is more comprehensive, intuitive and easy to implement in practical application. This study assumes the early warning effect of attitude angle on UAV to achieve accurate calculation and prediction of unmanned attitude angle and improve the working effect of UAV. The practical significance of this research lies in the realisation of automatic early warning of UAV attitude anomalies, which is conducive to the analysis and adjustment of UAV status by relevant personnel. In addition, the proposed model has broad application prospects in the fields of environmental detection and national defence security.

2 Related work

For the development of MEMS technology, scholars at home and abroad have conducted in-depth research on MEMS sensors and UAV attitude detection. A MEMS scale angular position sensor was presented by Bakhom (2022), and it offers several benefits over conventional variable capacitors of the same size. To increase the sensor's sensitivity and to get quicker response times and more accuracy, MEMS sensors may change huge capacitance. Mousavi et al. (2021) applied the electrostatic levitation force to the micro-electromechanical system. They discovered many different actuation mechanisms, demonstrated the viability of each one using MEMS sensors and pressure switches and confirmed via tests that the MEMS sensors are better at precisely detecting side-electrode contact force. Scholars such as Su et al. (2018) used MEMS gas sensors in the detection of inert gases, and designed an adapted topological structure. They found that the structure can respond to the mass loading effect. They found that the structure can respond to the mass load effect. In addition, the structure can make the inert gas react with metal oxide, thus generating conductivity, so as to realise the accurate detection of inert gas. Tina et al. (2021) used nanomechanical cantilever beam sensors in new ring-energy materials, which significantly improved the sensing performance. They found four curved suspended circular adsorption films in the MEMS structure, and then used high-precision four-point bending fixture experiments. The strain factor of ITO film was tested to achieve improved sensitivity and accuracy.

Reinhardt and Johansen (2021) proposed a predictive controller for a nonlinear model, which can control the quadratic cost of the UAV's three-axis angle to a minimum value. From the experimental results, this method has a strong Applicability and accuracy. Fan et al. (2022) created a self-focus mechanism and utilised the transformer network approach to identify rotor UAVs. This technique successfully raises the UAV identification algorithm's accuracy to a level that is 1.7 times higher than it was before the upgrade. Xu et al. (2019) used decision trees to establish a multi-model unscented Kalman filter attitude estimation method. This method uses quaternions to solve the attitude and uses decision trees to increase the anti-interference ability of the model. The experimental findings demonstrate the resilience and real-time estimate accuracy of the

attitude estimation approach. Ebrahimi et al. (2018) use Unmanned Aerial Vehicles (UAVs) to collect mobile phone data in dense wireless sensor networks, and use projected compressed data as a solution. It is shown via comparison studies that the suggested strategy and the created algorithm have certain benefits. Samir et al. (2020) adopted an online model-free deep reinforcement learning in the UAV-assisted Internet of Things network. This reinforcement learning can obtain the instantaneous channel status information of the UAV in real time and adjust the deployment height of the UAV. Meanwhile, MDP and PPO algorithms are used to solve the formulaic problem and finally achieve the timely transmission of data.

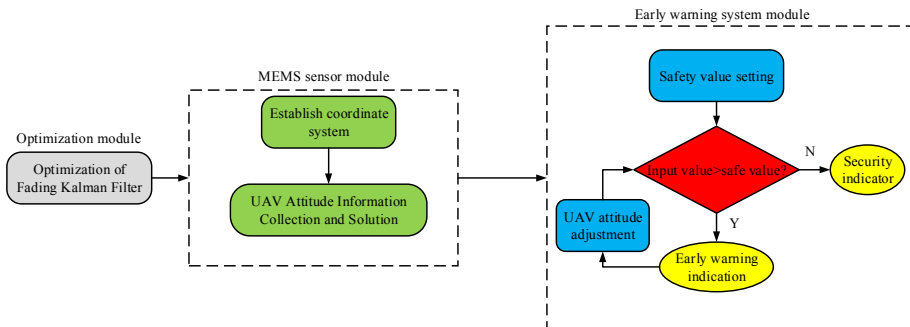
To sum up, MEMS sensors have high-detection accuracy and are widely used in various fields, especially in the field of unmanned aerial vehicles. However, there are few researches on using MEMS sensors to detect UAV attitude. Therefore, this study combines the two to optimise the MEMS sensor, and then analyses the impact of MEMS sensor on the performance of UAV attitude detection.

3 Gyro error compensation based on fading Kalman filter in MEMS sensor

3.1 UAV attitude angle measurement based on gyro output

The study proposes an automatic early warning model for UAV attitude abnormalities based on MEMS sensors. The model is mainly divided into three modules. The first module is MEMS sensor solution. The second module is MEMS sensor optimisation, and the third module is system early warning. After the MEMS sensor completes the data collecting and processing, it instantly communicates the data to the early warning system and then compares the provided data with the predetermined safety value, therefore accomplishing automated early warning. The specific structure of the model is shown in Figure 2.

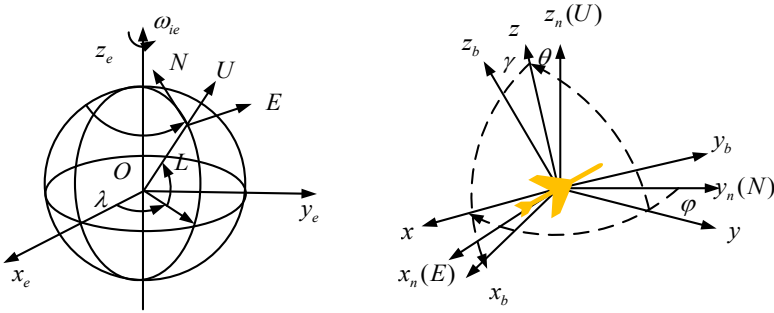
Figure 2 Structure of automatic early warning model for UAV attitude anomaly based on MEMS sensor



In Figure 2, different coordinate systems need to be established in the MEMS sensor module first, and there is relative motion between the coordinate systems. To solve the attitude of the UAV, it is first necessary to solve the coordinate system. The position

change of the UAV in the coordinate system is measured by the MEMS gyroscope. The study improves the accuracy of drone position changes by calculating the noise in the MEMS gyroscope using an Autoregressive Moving Average (ARMA) model and removing the noise using a fading Kalman filter. The abnormal attitude state of UAV can be judged by the rotation angle. The maximum inclination angle of UAV is 55° , and the safety critical value is set to 50° . When the detection value is greater than the safety value, the model will give an early warning. Therefore, in the navigation system, the calculation of the attitude angle of the carrier plays an important role. The carrier attitude angle computation uses the three-axis gyro signal to produce the attitude matrix. The calculated attitude matrix may be used to calculate the three rotation angles of the UAV coordinate system in the navigation system. First, a schematic diagram is established between relevant coordinate systems, as shown in Figure 3.

Figure 3 Relationship between established related coordinate systems



(a) Establishment of geographic coordinate system and earth coordinate system (b) Establishment of geographic coordinate system and airframe coordinate system

In Figure 3(a), the earth coordinate system and geographic coordinate system are established. The rotation between them is represented by the transfer of longitude λ and latitude L . In Figure 3(b), the body coordinate system and geographic coordinate system are established, which are represented by system b and system n respectively. Let the heading angle be φ ; the pitch angle be θ ; the roll angle be γ . The body coordinate system is generated by rotating the geographic coordinate system in various directions, according to the notion of attitude angle. There are three commonly used methods to solve UAV attitude angle, including Euler angle method, nine-parameter method and quaternion method (Peng et al., 2022; Bagheri et al., 2018; Peng et al., 2019). Among them, the Euler angle method and the nine-parameter method will generate a large amount of calculations during the calculation process, which does not meet the real-time performance. As a result, the quaternion method is chosen for UAV attitude solution. The quaternion method takes one coordinate system as the reference object, and the rotation relationship of another coordinate system or vector can be described by quaternion. The notion of attitude quaternion is taught using the quaternion method's properties. Assuming that the vector \bar{q} represents the attitude quaternion vector, and restricting the vector \bar{q} in $\bar{q} = [q_0, \mathbf{q}]^T$, the specific expression is shown in the formula (1).

$$\bar{q}^T \bar{q} = q_0^2 + \mathbf{q}^T \mathbf{q} = 1 \tag{1}$$

Formula (1) is the constraint of attitude quaternion vector. The superscript T is the conjugate of the quaternion; q_0 means a vector, and $q_0 = \cos \frac{\mu}{2}$; q also means a vector, and its value is calculated as shown in the formula (2).

$$q = iq_1 + jq_2 + kq_3 = \xi \sin \frac{\mu}{2} \quad (2)$$

Equation (2) represents the calculation form of vector, ξ represents the rotation axis of the vector; μ represents the rotation angle of the vector; i, j, k are all real numbers. The unit quaternion can represent the transformation relationship between the UAV coordinate system and the reference coordinate system. According to the vector rotation transformation relationship, the formula (3) is obtained.

$$r^n = \bar{q} \otimes r^b \otimes \bar{q}^{-1} \quad (3)$$

Formula (3) represents the rotation transformation relationship of vector, \otimes is used to represent the product calculation in the quaternion. As a result, the attitude matrix expressed by quaternion is shown in equation (4).

$$C_n^b(\bar{q}) = \begin{bmatrix} q_0^2 + q_1^2 - q_2^2 - q_3^2 & 2(q_1q_2 + q_0q_3) & 2(q_1q_3 - q_0q_2) \\ 2(q_1q_2 - q_0q_3) & q_0^2 - q_1^2 + q_2^2 - q_3^2 & 2(q_2q_3 + q_0q_1) \\ 2(q_1q_3 + q_0q_2) & 2(q_2q_3 - q_0q_1) & q_0^2 - q_1^2 - q_2^2 + q_3^2 \end{bmatrix} \quad (4)$$

Formula (4) represents the quaternion form of the attitude matrix, and the quaternion vector satisfies the differential equation, then there is formula (5).

$$\dot{\bar{q}} = 0.5\bar{q} \otimes \bar{\omega}_{nb}^b \quad (5)$$

In formula (5), $\bar{\omega}_{nb}^b$ represents the projection of rotational angular velocity of b system relative to n system in n system. If $\bar{\omega}_{nb}^b$ is expressed by quaternion, the expression of projection is shown in formula (6).

$$\bar{\omega}_{nb}^b = \begin{bmatrix} 0 & (\omega_{nb}^b)^T \end{bmatrix}^T \quad (6)$$

Bring formula (6) into the differential equation and expand to get formula (7).

$$\dot{\bar{q}} = \begin{bmatrix} \dot{q}_0 \\ \dot{q}_1 \\ \dot{q}_2 \\ \dot{q}_3 \end{bmatrix} = \frac{1}{2} \begin{bmatrix} q_0 \\ q_1 \\ q_2 \\ q_3 \end{bmatrix} \begin{bmatrix} 0 & -\omega_{nbx}^b & -\omega_{nby}^b & -\omega_{nbz}^b \\ \omega_{nbx}^b & 0 & \omega_{nbz}^b & -\omega_{nby}^b \\ \omega_{nby}^b & -\omega_{nbz}^b & 0 & \omega_{nbx}^b \\ \omega_{nbz}^b & \omega_{nby}^b & -\omega_{nbx}^b & 0 \end{bmatrix} \quad (7)$$

Formula (7) represents the quaternion differential equation; ω_{nbx}^b represents the x -axis angular rate value of the b system coordinate system; ω_{nby}^b represents the y -axis angular rate value of the b system coordinate system; ω_{nbz}^b represents the z -axis angular rate value of the b system coordinate system. The calculation technique for solving the matrix differential problem may be used to solve the quaternion differential equation.

The solution method is the Picard successive approximation method, and then the analytical formula of the quaternion differential equation can be obtained, as shown in formula (8).

$$q(q_t) = e^{\frac{1}{2} \int_0^t M^* (\omega_{nb}^b) dt} q(q_0) \quad (8)$$

Formula (8) represents the analytical expression of quaternion differential equation, M^* is the set of exponential integrals. Take the approximate value of the exponential integral formula to obtain the formula (9).

$$[\Delta\theta] = \int_0^t M^* (\omega_{nb}^b) dt = \begin{bmatrix} 0 & -\Delta\theta_x & -\Delta\theta_y & -\Delta\theta_z \\ \Delta\theta_x & 0 & \Delta\theta_z & -\Delta\theta_y \\ \Delta\theta_y & -\Delta\theta_z & 0 & \Delta\theta_x \\ \Delta\theta_z & \Delta\theta_y & -\Delta\theta_x & 0 \end{bmatrix} \quad (9)$$

In formula (9), $\Delta\theta_{x,y,z} = \frac{\omega_{nbx,y,z}^b \times T \cdot \pi}{180}$, and T represents the filter cycle. The transformation quaternion of coordinate system b obtained from coordinate system n can be determined by the rotation order of UAV triangle, and its specific expression is shown in Formula (10).

$$\begin{cases} q = q(-Z)q(X)q(Y) \\ q(-Z) = \cos \frac{\varphi}{2} - k \sin \frac{\varphi}{2} \\ q(X) = \cos \frac{\varphi}{2} + i \sin \frac{\varphi}{2} \\ q(Y) = \cos \frac{\gamma}{2} + j \sin \frac{\gamma}{2} \end{cases} \quad (10)$$

Formula (10) represents the rotation calculation of UAV in all directions, $q(-Z)$ represents the heading angle of the UAV and is negative; $q(X)$ represents the pitch angle of the UAV; $q(Y)$ represents the roll angle of the UAV. Therefore, if the corresponding equation is replaced in the formula (10), the functional relationship between the quaternion and the attitude angle can be obtained. The attitude angle may then be determined, and its calculation range is inside the inverse trigonometric function's primary value range, therefore the quadrant factor should also be included. According to the above analysis, the quaternion method can work with full attitude, and it is subject to fewer restrictions. Using this approach to solve linear differential equations ensures that the equation system has only four unknowns and reduces the length of work significantly. Furthermore, the calculating efficiency is increased.

3.2 MEMS gyro error analysis and compensation

The MEMS gyroscope is the essential technology in the UAV attitude measurement system, and the measurement precision of the gyroscope has a vital link with the UAV attitude. If you want to obtain high-precision UAV attitude information, it is essential to improve the UAV gyro measurement accuracy. As a result, this part investigates the

gyroscope error, develops the appropriate model, evaluates the error characteristics and finally adjusts for it. Gyro error includes systematic error and random error. The systematic error is the most important error source in gyro error. The random error is mainly caused by noise, and its size has a positive correlation with time. MEMS gyroscope output is composed of systematic error and random error, and its expression is as formula (11).

$$\omega_z = \omega + S_z \omega + B_f + n_z \tag{11}$$

In formula (11), ω represents the real angular velocity of the UAV; S_z represents the scale factor error; B_f represents the zero bias error; n_z represents the random drift. Among them are an effective calibration technique for compensating the B_f system fault and the zero-mean value of the static data for eliminating S_z . When researching random error compensation, an ARMA model can be chosen. This model is one of the standardised models of time series analysis. The autoregressive moving average model of this model is expressed in $ARMA(p, q)$, where p and q are the order of the model. Its general expression is shown in formula (12).

$$x_t + \phi_1 x_{t-1} + \phi_2 x_{t-2} + \dots + \phi_p x_{t-p} = w_t + \rho_1 w_{t-1} + \rho_2 w_{t-2} + \dots + \rho_q w_{t-q} \tag{12}$$

In formula (12), ϕ represents the coefficient of autocorrelation; ρ represents the moving average. The order of the model needs to be determined during the modelling process. The commonly used methods include Final Prediction Error Criteria (FPE) and Akaika Information Criterion (AIC). The order of gyro random error model is small. Therefore, in the actual system, the model generally adopts the moving average order less than or equal to the autoregressive order. Meanwhile, Moving Average (MA) and ARMA model parameters are estimated using the armax function, and the relevant AIC and FPE values are calculated (Haile et al., 2021; Dixit and Jayakumar, 2022). The criterion values of different models are shown in Table 1.

Table 1 Comparison of criterion values of different models

Criterion value	Model Type					
	ARMA(1,1)	ARMA(2,1)	ARMA(2,2)	MA(1)	MA(2)	MA(3)
FPE	0.0027	0.0021	0.0020	0.0091	0.0040	0.0023
AIC	-5.9756	-6.2433	-6.3727	-4.6987	-5.3895	-5.7941

The values of FPE and AIC should be based on the minimum principle, so the random drift model of the gyro $ARMA(2,1)$ is selected. The model parameters were fitted by the least squares method. Its specific expression is shown in formula (13).

$$x(k) = w(k) + 0.06791w(k-1) + 1.574x(k-1) - 0.7019x(k-2) \tag{13}$$

Equation (13) represents the fitting form of the state vector of gyro drift, $x(k)$ represents the state vector of gyro drift; $w(k)$ represents the white noise in the system. The contrast of the white noise is 0.0108, and the mean value of the white noise is 0, according to the residual signal of the residual information number that was calculated after choosing the

model fitting. After the model is determined, the research uses fading Kalman filter to compensate (Hu et al. 2018; Nazemipour and Manzuri 2018; Liu et al. 2021). Since the noise in the Kalman filter equation is all white noise, the noise of the studied system does not meet the conditions and the filter needs to be improved. The improvement measures can use the state expansion method (Sun et al. 2021; Manzoni et al., 2021). First, let $X = [x_k, x_{k-1}, \omega_k]^T$ be the state vector of the system, in which the angular rate sensitive by the gyro is represented by $\omega(k)$; the random error corresponding to the model is expressed in x_k . Then, the system state and measurement equation are shown in Formula (14).

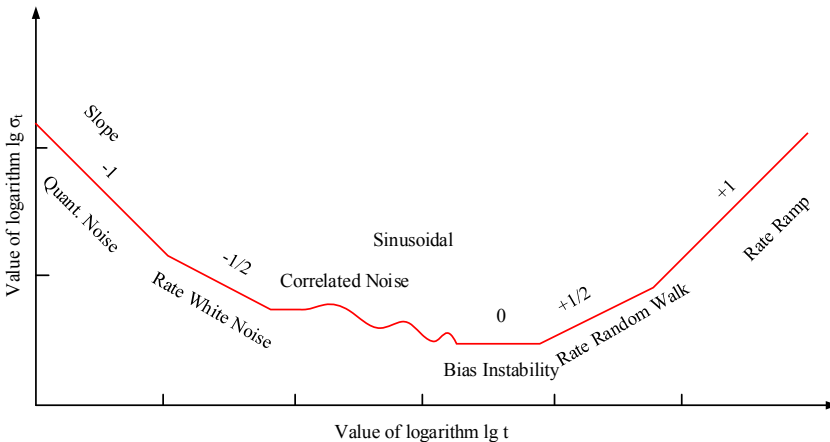
$$\begin{cases} \begin{bmatrix} X_k \\ \omega_k \end{bmatrix} = \begin{bmatrix} \phi_{k,k-1} & 0 \\ I & 1 \end{bmatrix} \begin{bmatrix} X_{k-1} \\ \omega_{k-1} \end{bmatrix} + \begin{bmatrix} I \\ 0 \end{bmatrix} W_{k-1} \\ Z_k = H_k X_k + V_k \end{cases} \quad (14)$$

In formula (14), Z_k represents the observed value of the system; V represents the variance of the observed signal under static conditions, its mean value is 0 and the value is 0.0275; H_k represents a time-varying matrix; I represents the identity matrix. The attitude angle error of the UAV before and after filtering can be obtained by formula (14). Five inertial measurement module defects – rate ramp R , flicker noise B , quantisation noise Q , angular rate random walk K and angle random walk N – make up the majority of gyro random errors. In the analysis of the random error of the gyroscope, the Allan variance method is recognised by IEEE as a standard method for random error testing (Maddipatla et al., 2021; Hofmann and Knopp 2022). The formula (15) can be obtained by integrating the Allan variance of the five random errors.

$$\sigma^2(t) = \frac{N^2}{t} + \frac{R^2 t^2}{2} + \frac{2B^2}{\pi} \ln 2 + \frac{K^2 t}{3} + \frac{3Q^2}{t^2} \quad (15)$$

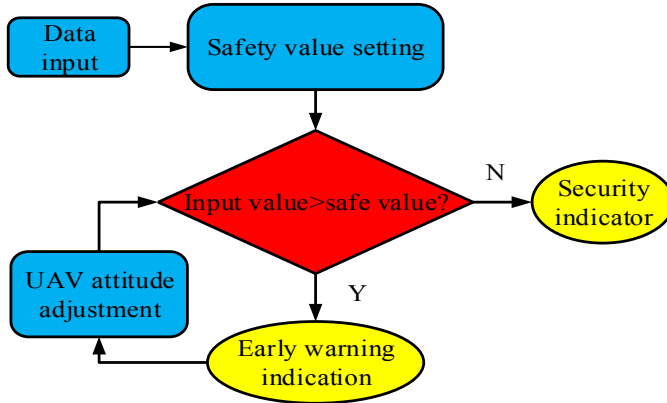
In formula (15), $\sigma^2(t)$ is the expression of Allan variance. The Allan technique curve is created using formula (14), as shown in Figure 4.

Figure 4 Sample of Allan variance double logarithm curve



In Figure 4, according to the length of the time series, the Allan variance can accurately identify the noise ratio and noise source, which is of great significance for improving the detection accuracy of drones. After determining the optimisation method of the second module of the model, the early warning module is constructed. The flow chart of the early warning module is shown in Figure 5.

Figure 5 Flow chart of early warning model



Setting a safe value for the UAV attitude deflection angle in the early warning module is the major way to achieve real-time early warning of UAV attitude abnormality. The model will provide an early warning indication when the input value of the MEMS sensor exceeds the safe value; when the input value is less than the safe value, the model shows a normal indication.

3.3 Model experiment environment and parameter settings

In the experiment, the medium-precision MEMS inertial sensor ADIS16405 produced by ADI Company was selected as the measurement unit; a three-axis turntable model AS-0011 was used for dynamic and static experiments. In the performance analysis of UAV attitude detection, the scale error of the selected level instrument is 0.02 mm/lm, and the initial value of the state selected by the Kalman filter is $X_0 = [0 \ 0 \ 0]^T$.

As an important parameter, the random error of MEMS gyroscope needs to be determined in advance. The experimental turntable is used to obtain the bias data of the x -axis, y -axis and z -axis of the MEMS gyroscope. After that, the bias data is processed in blocks, and the average value after processing is totalled by the square difference. Then, as illustrated in Figure 6, create the equivalent Allan variance log-log curve based on the total.

Figure 6 Allan variance double logarithm curve in three axis direction

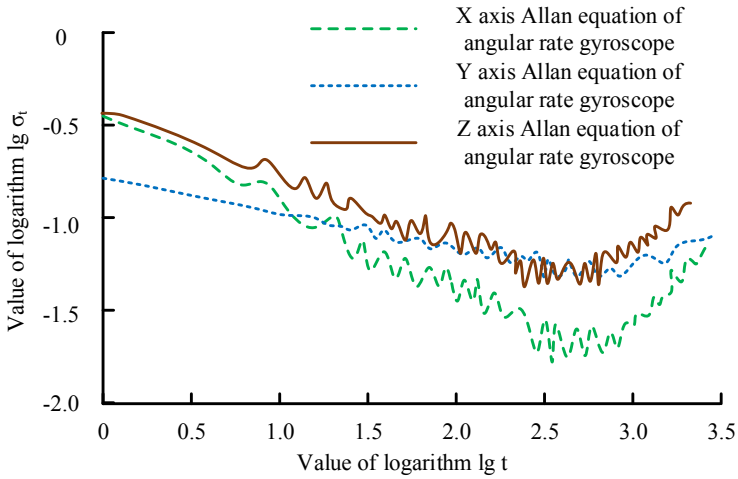


Figure 6, the abscissa is the value of $\lg t$; the ordinate is the value of $\lg \sigma_t$. The value of each noise factor for the MEMS gyroscope may be calculated using the formula (15) and the least squares approach of fitting the Allan variance double-logarithmic curve. The error coefficients obtained by the MEMS gyroscope according to different axes are shown in Table 2.

Table 2 Error coefficient of MEMS gyroscope according to different axes

Noise figure	<i>x</i> -axis	<i>y</i> -axis	<i>z</i> -axis
<i>Q</i>	0.0239	0.0108	0.1325
<i>N</i>	0.1382	0.0142	0.1037
<i>B</i>	0.3082	0.2175	0.3581
<i>K</i>	0.7382	0.6218	0.9513
<i>R</i>	0.0182	0.0032	0.0203

Seen from the data in Table 2, the coefficients of the angular rate walk error in the three axes are the largest, and they are 0.7382, 0.6218 and 0.9513 in the *x*-axis, *y*-axis and *z*-axis, respectively; the following are the flicker-induced error coefficients, respectively 0.3082, 0.2175, 0.3581; the remaining three error coefficients account for a small proportion. Therefore, it has been convincingly shown that the MEMS gyro error term exhibits both the first-order Markov process and continuous drift. As a result, the variance of the model's random drift white noise is $5^\circ/h$, and the first-order Markov process noise's mean square error is 0.0002 g.

4 Analysis of detection effect of UAV attitude abnormal state based on MEMS sensor

4.1 Performance analysis before and after MEMS gyroscope filtering

The calculation form and parameter type of the model have been determined. Now the model parameters and performance are determined by experiment. Firstly, the performance of the improved filter is analysed to determine the prediction accuracy of the model under static and dynamic conditions. The research contrasts the fading Kalman filter’s error impact with the sine wave’s normal condition in a traditional Kalman filter. In the dynamic and static experiments of the conventional Kalman filter, the initial values are selected according to the parameters. The resulting static filtering graph is shown in Figure 7.

Figure 7 Kalman static filtering graph

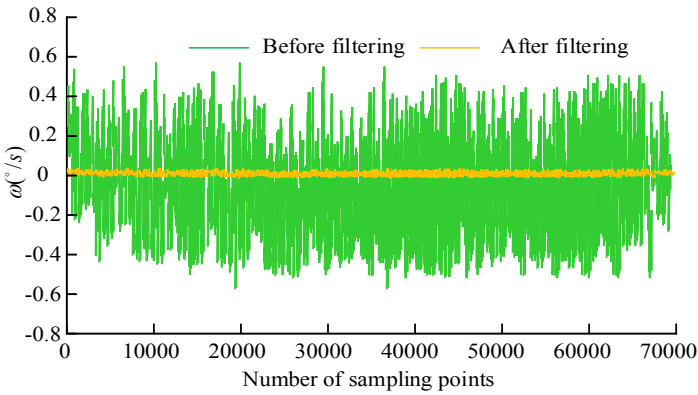


Figure 7 shows the static filtering graph obtained by conventional Kalman filter. The error standard deviation before filtering is 0.1901(°/s), and the error standard deviation after filtering is 0.0070(°/s), which is 3.682% of that before filtering. Therefore, it can be judged that under static conditions, the random error of the gyroscope can be greatly reduced through the Kalman filter, which significantly improves the measurement accuracy of the gyroscope. Place the system on a three-axis turntable, control the angular speed of the turntable at 20°/s, 40°/s and 60°/s, respectively, and analyse the x-axis of the angular rate gyro. According to the difference in angular rate, the corresponding results before and after filtering are obtained and the comparison of the results is shown in Table 3.

Table 3 Mean value and standard deviation of errors before and after filtering at different angular rates

Angular rate (°/s)	Mean value of error (°/s)		Standard deviation of error (°/s)	
	Before filtering	After filtering	Before filtering	After filtering
20	-0.3312	-0.1013	0.2412	0.0102
40	-0.3233	-0.0962	0.4243	0.0124
60	-0.3624	-0.1023	0.3314	0.0108

Table 3 demonstrates that when the angular rate is constant. The changes of the error mean value and error standard deviation before and after filtering are less different from those in the static experiment. Because of this, even while the traditional Kalman filter may also lower the gyroscope's random error in the situation of constant angular rate, the gyroscope's measurement accuracy can be enhanced to a certain degree. However, in reality, it is impossible for the gyroscope to remain stationary or keep moving at a constant angular rate. When the UAV is in motion, the angular rate values at each moment change differently. In this case, the conventional Kalman filter is used to obtain the effect shown in Figure 8.

Figure 8 Effect diagram of Kalman filter when the angular rate changes

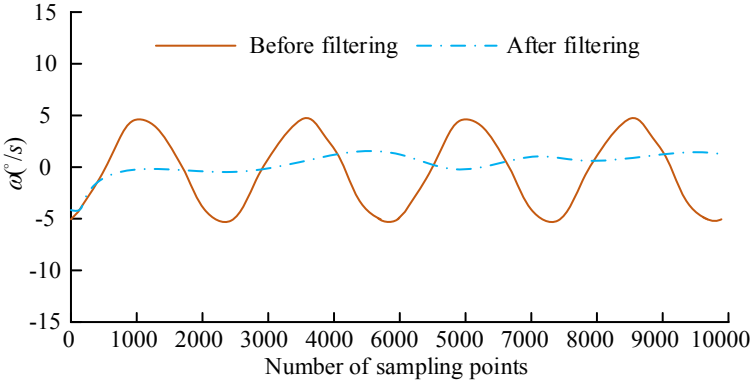


Figure 8 shows that before filtering, it is in a state of sine wave oscillation and its angular rate changes momentarily in the interval $[-5^\circ/s, 5^\circ/s]$. The output value of the MEMS gyroscope has a large error after filtering, which cannot accurately reflect the angular rate of the gyroscope. In view of this situation, the study uses the fading Kalman filter for comparison. In addition, in the state of sine wave oscillation, the fading Kalman filter is used to obtain the effect diagram in Figure 9.

Figure 9 Effect diagram of fading Kalman filter when the angular rate changes

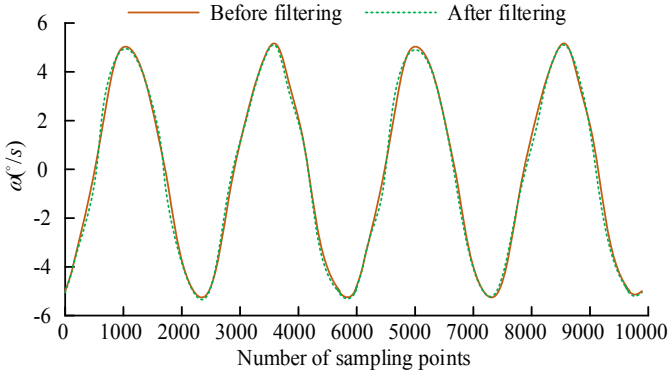


Figure 9 depicts the fading Kalman filter’s sine wave oscillation condition both before and after filtering. Figure 9 shows that the fading Kalman filter’s sine wave oscillation range before and after filtering is in the range $[-5^\circ/s, 5^\circ/s]$, and that the sine wave oscillation is more stable and the error produced is reduced. The results demonstrate that even when the angular rate value varies, the fading Kalman filter still has a decent tracking effect.

4.2 Static and dynamic experimental performance analysis of attitude measurement simulation system

The attitude of the UAV is discovered and examined after the MEMS gyroscope’s performance in static and dynamic states is examined, both before and after filtering. The experiment’s mean error and mean square error serve as indicators of detection accuracy. The difference between the projected attitude and the actual attitude is a good indicator of how accurate early warning is. Firstly, the static heading and attitude of the UAV are measured and analysed in the experiment: the three axes of the AS-0011 turntable and the three axes of the measuring unit are kept coincident; the level meter is levelled and zeroed according to the turntable; then a 200 s static experiment is carried out. The output curves of filtered pitch angle, roll angle and heading angle can be obtained through the above operations, as shown in Figure 10.

Figure 10 Results of filtered attitude angle output curve in UAV static experiment

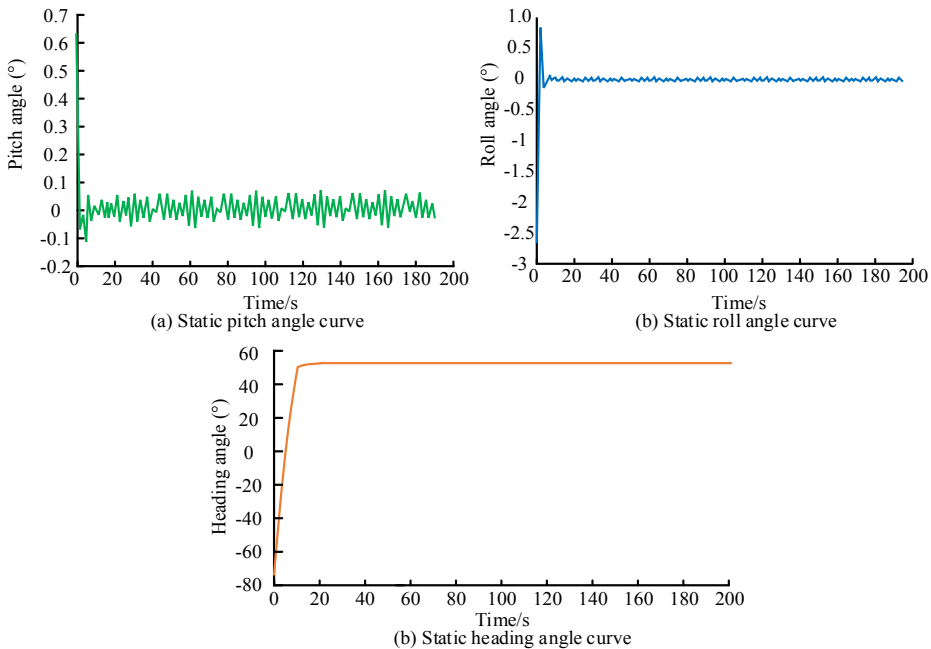
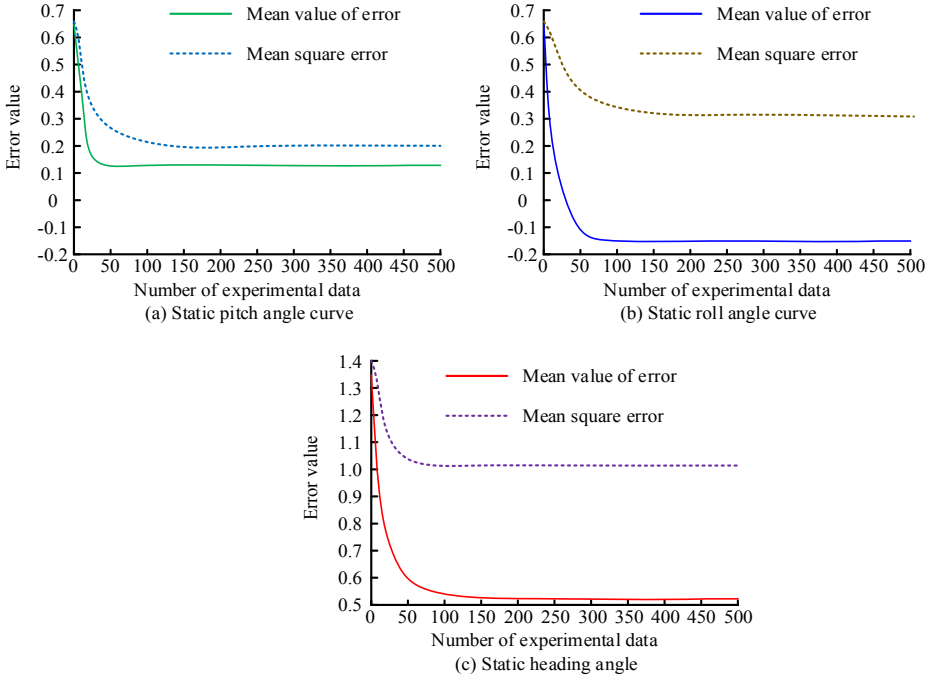


Figure 10 shows the analysis results of UAV heading and attitude system in static experiment. In Figure 10(a), after the experiment lasted for about 4 s, the pitching angle of the UAV tended to be stable and its variation value was between -0.1° and 0.1° . In Figure 10(b), the degree of change of the roll angle of the UAV also tends to be stable at

about 4 s, and its change value changes in the range of plus or minus 0.05° . In Figure 10(c), the change of UAV's heading angle is stable after 8 s, and it is stable at about 52° . It demonstrates that, even when static unmanned motion accelerates, the UAV's heading and attitude system has a quick convergence rate and does not diverge.

Figure 11 Attitude error results of UAV attitude measurement system in static state



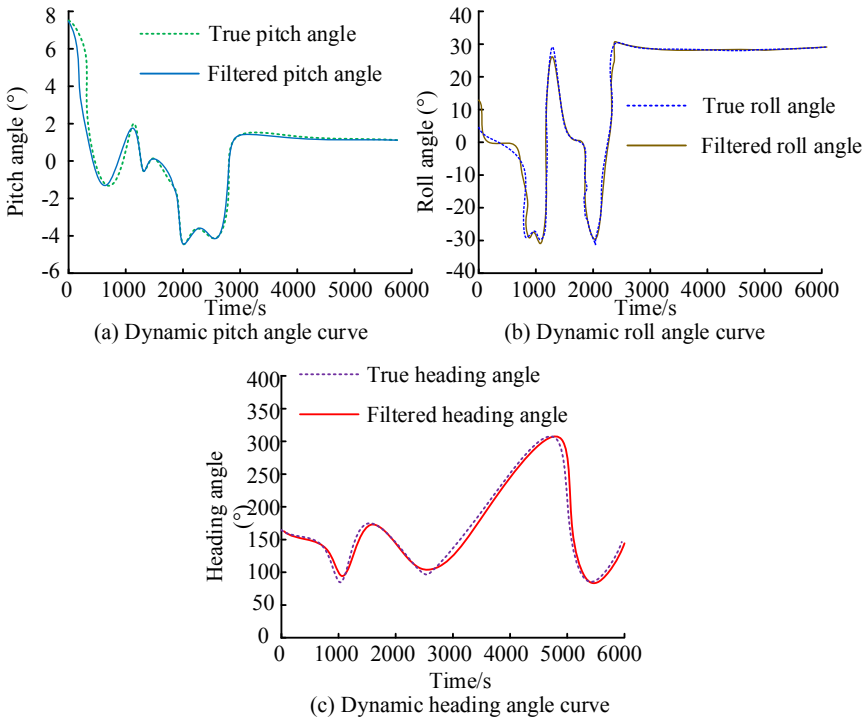
In the static experiment, the experiment collected the data of 500 times of static experiment and the attitude data output by the attitude system measurement, and performed error analysis on it. The results are shown in Figure 11. In Figure 11(a), the mean error of UAV pitch angle detection tends to be stable after 25 experiments, the mean error is about 0.12° , and the mean square error is about 0.20° . In Figure 11(b), the UAV error of the roll angle tends to be stable after 50 experiments. The mean error is about -0.16° , and the mean square error is about 0.31° . In Figure 11(c), the error of the UAV heading angle detection tends to be more stable. The mean error is about 0.50° , and the mean square error is about 1.03° . The attitude system performs better at error detection in static trials, according to an examination of the total error data. The UAV's heading angle error, which is the consequence of mistakes brought on by things like magnetic media, is roughly 0.5° , while the pitch angle and roll angle faults are also within 0.2° . Therefore, the attitude system has high-detection accuracy in the static state. When the attitude of the UAV is about to be abnormal, it can detect and give an early warning at the first time.

A three-axis turntable is employed in the dynamic experiment to replicate the highly manoeuvrable flying condition of the UAV. The three-axis turntable is attached with the UAV attitude measuring equipment during the experiment. The system filtering performance and attitude angle calculation accuracy are examined by contrasting the

estimated attitude angle of the system with the actual attitude angle of the turntable experiment. The initial attitude angle of the UAV is measured experimentally: the pitch angle is 7.7° ; the roll angle is 0° ; the heading angle is 149° . The experiment time is set to 60,000 s.

Figure 12 is the comparison result between the obtained system attitude angle curve and the real attitude angle. The filter is shown in an unstable condition in Figure 12(a) when the system first begins to operate, and in this state there are several crossings between the attitude value line type calculated by the system and the real value line type. But at about 100 s, the line patterns began to overlap, indicating that there was a small error between the attitude estimation of the system and the real attitude at that moment. Figure 12(b) illustrates how, when the UAV issues a right turn instruction, the roll angle quickly changes, going from -35 to 35° in a short period of time, yet the filtered roll angle continues to be very similar to the real roll angle. In Figure 12(c), the system can realise all-round attitude tracking in the heading angle, and can also realise smooth transition at the critical point.

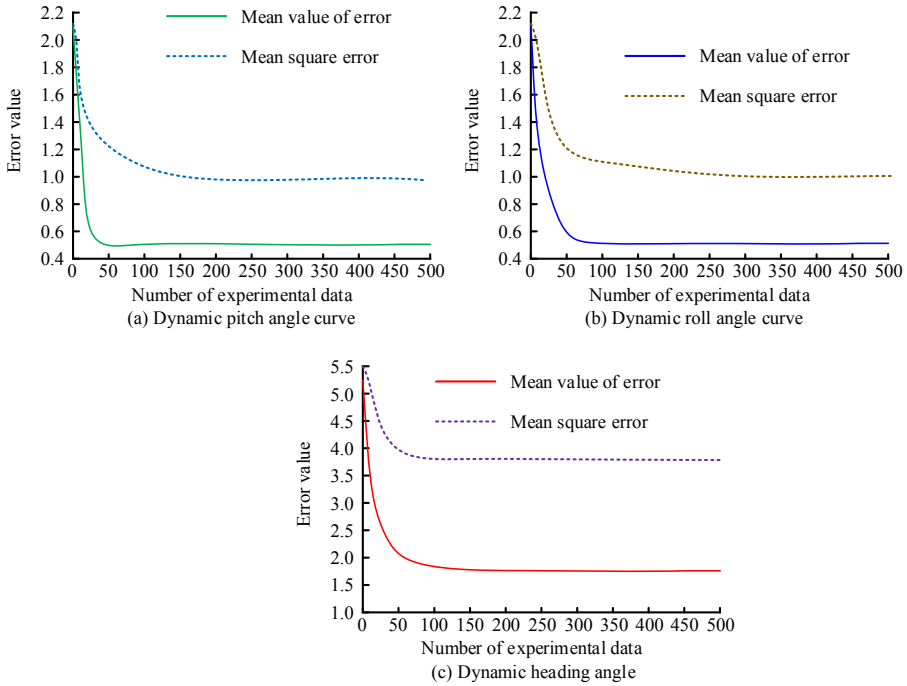
Figure 12 Comparison results of system attitude angle curve and real-attitude angle



500 sets of experimental data were gathered for the turntable experiment in the high manoeuvring condition of the UAV, and the attitude angle errors of the two were compared and examined. Figure 13 shows the attitude error diagram in the dynamic experiment. In Figure 13(a), the detection error of the pitch angle tends to be stable after 30 experiments. The mean error is about 0.49° , and the mean square error is about 0.99° . In Figure 13(b), the detection error of the roll angle tends to be stable after 50 trials. The

mean error is about 0.52° , and the mean square error is about 1.00° . In Figure 13(c), the detection error of heading angle tends to be stable after 75 trials. The mean error is 1.80° , and the mean square error is about 3.8° . In terms of the overall error findings, the UAV's pitch and roll angle errors are both under 0.5° , and the average heading angle error is kept to within 2° . The experiment validates the validity of the early warning model for the abnormal condition of the UAV suggested in the research, and the findings demonstrate that the attitude detection of the UAV still has good detection accuracy in the state of high mobility.

Figure 13 Attitude error results of UAV attitude measurement system in high manoeuvre state



5 Conclusion

The advancement of UAV technology has increased along with the constant advancement of microelectronics technology, and it is now extensively used. However, in the practical application of UAV, the problem of abnormal attitude often occurs, which leads to the damage of UAV. As a result, it is crucial to find and warn about UAV attitude anomalies as soon as possible. In this experiment, an automatic early warning model of UAV attitude anomaly was established. The simulation results show that in the system static simulation experiment, the MEMS sensor compensated by the fading Kalman filter can predict the three-axis angle of UAV with high accuracy in a short time, and the average prediction error of the three-axis angle is 0.127° , -0.163° and 0.513° , respectively; In the experiment of high manoeuvrability, the prediction of MEMS sensors can still be highly consistent with the actual situation and their three-axis angular errors

are within 2° , 0.490° , 0.524° and 1.820° , respectively. To address the issue of the MEMS gyroscope's poor accuracy, an Allan variance analysis of the gyroscope error is performed, and the impact of each mistake item on the random error of the gyroscope is examined. In order to improve the measurement accuracy of MEMS gyroscope, the ARMA (2,1) model of random drift of gyroscope is constructed experimentally. In this regard, Kalman fading Kalman filter is used to compensate the random drift error of gyroscope in the experiment, which solves the problem of poor compensation effect of traditional filter. The proposed method can greatly improve the detection accuracy of sensors, and can realise real-time and effective early warning of UAV attitude anomalies. However, there are still shortcomings in the research. For instance, in the simulation experiment, the effects of the weather, temperature and magnetic field on UAV are not simulated. Aiming at further improving the attitude prediction of UAVs in actual environments, future study may examine the application impact of MEMS sensors in various weather, temperature and magnetic field intensity conditions.

References

- Bagheri, K., Sadeghi, M.R. and Panario, D. (2018) 'A non-commutative cryptosystem based on quaternion algebras', *Designs, Codes and Cryptography*, Vol. 86, No. 10, pp.2345–2377.
- Bakhoun, E.G. (2022) 'MEMS-scale angular position sensor based on ultracapacitor technology', *Journal of Microelectromechanical Systems: A Joint IEEE and ASME Publication on Microstructures, Microactuators, Microsensors, and Microsystems*, Vol. 31, No. 2, pp.298–304.
- Bhole, K.S. (2022) ORCID. Available online at: <https://orcid.org/0000-0002-7466-2213>
- Bhole, K.S. and Kale, B. (2022) 'Sublimation technique for minimization of stiction induced during fabrication of closely spaced microstructures', *Advances in Materials and Processing Technologies*, Vol. 4, No. 8, pp.3889–3899.
- Dixit, S. and Jayakumar, K.V. (2022) 'A non-stationary and probabilistic approach for drought characterization using trivariate and pairwise copula construction (PCC) model', *Water Resources Management*, Vol. 36, No. 4, pp.1217–1236.
- Ebrahimi, D., Sharafeddine, S., Ho, P.H. and Assi, C. (2018) 'UAV-aided projection-based compressive data gathering in wireless sensor networks', *IEEE Internet of Things Journal*, Vol. 6, No. 2, pp.1893–1905.
- Fan, Y., Li, O. and Liu, G. (2022) 'An object detection algorithm for rotary-wing UAV based on AWin transformer', *IEEE Access*, Vol. 10, pp.13139–13150.
- Haile, E.A., Worku, G.B., Beyene, A.M. and Tuka, M.B. (2021) 'Modeling of doubly fed induction generator based wind energy conversion system and speed controller', *Journal of Energy Systems*, Vol. 5, No. 1, pp.46–59.
- Hofmann, C.A. and Knopp, A. (2022) 'Phase noise limits in low-rate communication via satellite', *IEEE Internet of Things Journal*, Vol. 9, No. 16, pp.14867–14875.
- Hu, G., Wang, W., Zhong, Y., Gao, B. and Gu, C. (2018) 'A new direct filtering approach to INS/GNSS integration', *Aerospace Science and Technology*, Vol. 77, pp.755–764.
- Li, M., Zhou, Z., Yi, L., Wang, X. and Adnan, S. (2019) 'Design of a test structure based on chevron-shaped thermal actuator for in-situ measurement of the fracture strength of MEMS thin films', *Nanotechnology and Precision Engineering*, Vol. 2, No. 4, pp.163–168.
- Liu, Y., Xu, Q., Sun, J., Shen, F. and Cuil, D. (2021) 'Vehicle state estimation based on strong tracking central different Kalman filter', *Mathematical Problems in Engineering: Theory, Methods and Applications*, Vol. 34, pp.4126961.1–4126961.20.

- Maddipatla, S.P., Haeri, H., Jerath, K. and Brennanl, S. (2021) 'Fast allan variance (FAVAR) and dynamic fast allan variance (D-FAVAR) algorithms for both regularly and irregularly sampled data', *IFAC-PapersOnLine*, Vol. 54, No. 20, pp.26–31.
- Manzoni, E., Rampazzo, M. and Favero, S.D. (2021) 'Detection of glucose sensor faults in an artificial pancreas via whiteness test on Kalman filter residuals', *IFAC-PapersOnLine*, Vol. 54, No. 7, pp.274–279.
- Mousavi, M., Alzgoool, M. and Towfighian, S. (2021) 'A MEMS pressure sensor using electrostatic levitation', *IEEE*, Vol. 21, No. 17, pp.18601–18608.
- Nazemipour, A. and Manzuri, M.T. (2018) 'MEMS gyroscope raw data noise reduction using fading memory filter', *Journal of Scientific and Industrial Research*, Vol. 77, No. 10, pp.553–558.
- Peng, T., Zhong, J., Tu, Z., Lu, J. and Lou, J. (2022) 'Finite-time synchronization of quaternion-valued neural networks with delays: a switching control method without decomposition', *Neural Networks: The Official Journal of the International Neural Network Society*, Vol. 148, pp.37–47.
- Peng, X., Shi, X. and Gong, Y. (2019) 'Dual-quaternion-based modeling and control for motion tracking of a tumbling target', *Journal of Systems Engineering and Electronics*, Vol. 5, pp.985–994.
- Reinhardt, D. and Johansen, T.A. (2021) 'Control of fixed-wing UAV attitude and speed based on embedded nonlinear model predictive control', *IFAC-PapersOnLine*, Vol. 54, No. 6, pp.91–98.
- Samir, M., Assi, C., Sharafeddine, S. and Ghayeb, A. (2020) 'Online altitude control and scheduling policy for minimizing AoI in UAV-assisted IoT wireless networks', *IEEE Transactions on Mobile Computing*, Vol. 7, No. 21, pp.2493–2505.
- Stepanovsky, M.A. (2019) 'Comparative review of MEMS-based optical cross-connects for all-optical networks from the past to the present day', *Communications Surveys and Tutorials*, Vol. 21, No. 3, pp.2928–2946.
- Su, A., Tcb, A. and Au, B. (2018) 'Design and simulation of MEMS gas sensor topologies for detection of inert Gases – ScienceDirect', *Materials Today: Proceedings*, Vol. 5, No. 10, Part 1, pp.21355–21362.
- Sun, T., Wu, R., Cui, Y. and Zhengl, Y. (2021) 'Sequent extended Kalman filter capacity estimation method for lithium-ion batteries based on discrete battery aging model and support vector machine', *Journal of Energy Storage*, Vol. 39, pp.102594.1–102594.11.
- Tina, B.S., Joel, Z., Rao, R.S.S. and Seena, V. (2021) 'Silicon MEMS nanomechanical membrane flexure sensor with integrated high gauge factor ITO', *Journal of Microelectromechanical Systems: A Joint IEEE and ASME Publication on Microstructures, Microactuators, Microsensors, and Microsystems*, Vol. 30, No. 6, pp.939–949.
- Xu, X., Tian, X., Zhou, L. and Li, Y. (2019) 'A decision-tree based multiple-model UKF for attitude estimation using low-cost MEMS MARG sensor arrays', *Measurement*, Vol. 135, pp.355–367.
- Ye, B-Y., Song, C-K., Huang, H., Li, Q.B., An, C-W. and Wang, J-Y. (2020) 'Direct ink writing of 3D-Honeycombed CL-20 structures with low critical size', *Defense Technology*, Vol. 16, No. 3, pp.588–595.